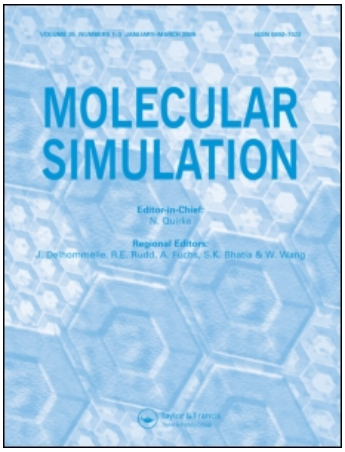

Molecular Simulation
Publication details, including instructions for authors and subscription information:
http://www.informaworld.com/smpp/title~content=t713644482

Effect of surface roughness on slip flows in hydrophobic and hydrophilic microchannels by molecular dynamics simulation

S. C. Yang[a]; L. B. Fang[a]
[a] Department of Mechanical Engineering, ChienKuo Technology University, Changhua, Taiwan, ROC

To cite this Article Yang, S. C. and Fang, L. B.(2005) 'Effect of surface roughness on slip flows in hydrophobic and hydrophilic microchannels by molecular dynamics simulation', Molecular Simulation, 31: 14, 971 — 977
To link to this Article: DOI: 10.1080/08927020500423778
URL: http://dx.doi.org/10.1080/08927020500423778

Molecular Simulation, Vol. 31, No. 14–15, 15–30 December 2005, 971–977

Effect of surface roughness on slip flows in hydrophobic and hydrophilic microchannels by molecular dynamics simulation

S. C. YANG* and L. B. FANG

Department of Mechanical Engineering, ChienKuo Technology University, Changhua 50094, Taiwan, ROC

(Received October 2005; in final form October 2005)

The influences of surface roughness on the boundary conditions for a simple fluid flowing over hydrophobic and hydrophilic surfaces are investigated by molecular dynamics (MD) simulation. The degree of slip is found to decrease with surface roughness for both the hydrophobic and hydrophilic surfaces. The flow rates measured in hydrophobic channels are larger than those in hydrophilic channels with the presence of slip velocity at the walls. The simulation results of flow rate are correlated with the theoretical predictions according to the assumption of no slip boundary condition. The slip boundary condition also strongly depends on the shear rate near the surface. For hydrophobic surfaces, apparent fluid slips are observed on smooth and rough surfaces. For simple fluids flowing over a hydrophobic surface, the slip length increases linearly with shear rate for both the smooth and rough surfaces. Alternately, the slip length has a power law dependence on the shear rate for the cases of hydrophilic surfaces. It is observed that there is a no-slip boundary condition only when shear rate is low, and partial slip occurs when it exceeds a critical level.

Keywords: Molecular dynamics; Slip; Surface roughness; Hydrophobic; Hydrophilic

1. Introduction

Hydrodynamic behaviors in microscale and nanoscale flows are quite different from those in macroscopic flows. The confined fluids of a nanoscale system are characterized by large surface-to-volume ratios, so that the influence of boundary conditions on the flow becomes significantly important. The applications of related systems include microfluidic devices, micro-electro-mechanical systems (MEMS), as well as fluid flow in nanoporous and in biological systems. It is well known that fluids flowing along a solid surface can undergo slip at the wall–fluid interface and the standard assumptions of the classical continuum theory with a no-slip boundary condition can break down. The wall slip can strongly influence the hydrodynamic behaviors in microscale and nanoscale flows. The phenomena of wall slip become important when the length scale over which the fluid velocity changes approaches the slip length

The parameter of slip length δ, is generally characterized to quantify the degree of slip, which is defined as the distance beyond the surface where the fluid velocity extrapolates to zero. The slip length is expressed as, $u_s = \delta(\partial u/\partial z)$, where u_s is the slip velocity at the surface. $\partial u/\partial z$ is the local shear rate and the z axis is perpendicular to the surface. From a theoretical point of view, the parameters controlling the degree of slip are still largely unknown. The degree of wall slip is highly dependent on the shear rate, the solid–fluid interaction energy or the wetting surface and the surface roughness. Although, in recent years the slip phenomena for Newtonian fluids have received much attention by means of experiments [1–11] and simulation [12–19], the understanding of the slip mechanism remains largely incomplete. Pit *et al.* [1] experimentally measured the flow velocity of a Newtonian fluid near a solid surface by following the movement of a photobleached test section, demonstrating that slip depends on both the fluid-wall interactions and the surface roughness. Zhu and Granick [2] directly measured the hydrodynamic drainage forces for Newtonian liquids by surface force apparatus (SFA), showing that the boundary slip is strongly dependent on the velocity gradient. Craig *et al.* [3] measured the hydrodynamic drainage force for a sphere approaching

*Corresponding author. Tel: +886-4-7111111. Ext. 3168. Fax: +886-4-7111137. Email: scyang@cc.ctu.edu.tw

Molecular Simulation
ISSN 0892-7022 print/ISSN 1029-0435 online © 2005 Taylor & Francis
http://www.tandf.co.uk/journals
DOI: 10.1080/08927020500423778

a flat wall in an aqueous Newtonian fluid. They concluded that the degree of wall slip depends on the surface approach velocity of the sphere and fluid viscosity. Tretheway and Meinhart [4] used micro particle image velocimetry to measure velocity profiles of water flowing through rectangular glass microchannels, demonstrating a significant fluid velocity near a hydrophobic surface and no slip for a hydrophilic surface. Tyrell and Attard [5] and Steitz *et al.* [11] experimentally observed the nanobubbles on hydrophobic surfaces by atomic force microscopy (AFM), and concluded that the presence of nanobubbles can result in significant boundary slip. Since the experimental observation of wall slip is extremely difficult, numerical simulations based on molecular dynamics (MD) offer a natural tool to investigate the phenomenon of slip boundary conditions for simple or polymeric fluids flowing through the solid surface. Employing MD simulation, Bocquet and Barrat and Bocquet [14] and Cieplak *et al.* [17] explored the dependence of the slip length on the wettability of the solid surface. They demonstrated that the slip length is controlled by the fluid–wall interaction energy and the fluid density between two solid walls. The relationships between shear rate and the degree of slip in Couette flow have been examined by MD simulation for both simple [13] and polymeric fluids [21]. The simulation results show that the slip length is shear independent at low shear rate and increases rapidly at higher shear rate for both simple and polymeric fluids. Sokhan *et al.* [19] carried out simulations of simple fluids undergoing steady-state poiseuille flow. They demonstrated that the fluid flow in carbon nanopores was characterized by a large slip length. However, there have been relatively few studies to quantify the influence of surface roughness on the magnitude of slip. Since few surfaces are smooth at the molecular scale, the influence of surface roughness on the degree of slip is important [20]. Some experimental studies have shown that the surface roughness either increases [6] or decreases [11] the degree of slip. Using MD simulation, Cottin-Bizonne *et al.* [18] have shown that the degree of wall slip is strongly affected by the surface roughness and is a function of pressure for a non-wetting patterned surface. They demonstrated that the slip length is enhanced at a "super-hydrophobic" state and a no slip boundary condition is found at a "normal" state. Galea and Attard [22] used MD simulation to investigate the magnitude of slip length in a shear flow. They showed that the slip phenomenon occurred for both smooth and rough surfaces, and that the degree of slip increased with the surface roughness. In this study, MD simulation is used to investigate the hydrodynamic behaviors and the boundary slip phenomena with surface roughness on an atomic scale in hydrophilic and hydrophobic surfaces. The dependence of wall slip velocity and flow rate is also investigated in detail. The simulation results are also compared with the theoretical predictions.

2. Simulation method

MD simulation is performed to investigate the flow behaviors and boundary slip of simple fluids in hydrophobic and hydrophilic microchannels in this study. Figure 1 shows the geometry of simple fluids confined between two parallel solid walls. The two parallel walls are in the x–y plane. The distance between the first layer of the solid walls $L_z = 10\sigma$ and the lateral cell dimensions $L_x \times L_y = 20\sigma \times 10\sigma$. The periodic boundary conditions are applied in the x and y directions. For a fluid, the velocity $\mathbf{v}_i$ and the momentum $\mathbf{P}_i$ of molecule i are given by

$$\mathbf{v}_i = \frac{\mathbf{p}_i}{m} \tag{1}$$

$$\dot{\mathbf{P}}_i = \sum_{j \neq i} \mathbf{F}_{ij} + \mathbf{F}_{\mathrm{e}} \tag{2}$$

where m is the mass of the fluid molecule, $\mathbf{F}_{ij}$ is the intermolecular force of molecule i due to molecule j and $\mathbf{F}_{\mathrm{e}}$ is the external driving force. An external force in the x direction is applied to drive the fluid atoms in the simulation. The mass of wall molecules, m_{f}, is assumed to be identical to that of fluid molecules and the equations of motion for wall molecules are similar to equation (2), except that the external force is now replaced by the spring force. For both the fluid and wall molecules, the Lennard–Jones (L–J) potential function is used to calculate the intermolecular force. The L–J potential for fluid molecules is given by

$$u(r_{ij}) = \begin{cases} 4\varepsilon_{\mathrm{f}}\left[\left(\frac{\sigma_{\mathrm{f}}}{r_{ij}}\right)^{12} - \left(\frac{\sigma_{\mathrm{f}}}{r_{ij}}\right)^{6}\right] & r_{ij} \leq r_{\mathrm{c}} \\ 0 & r_{ij} \geq r_{\mathrm{c}} \end{cases} \tag{3}$$

where r_{ij} is the distance between particle i and j, ε_{f} represent the energy parameter, σ_{f} is the diameter of fluid molecular and r_{c} is the cutoff distance, which is equal to $2.5\sigma_{\mathrm{f}}$. The interaction forces between fluid and wall

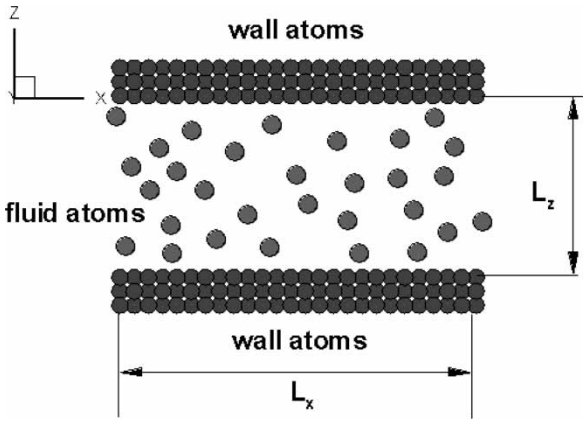

Figure 1. Schematic of simple fluids confined between two parallel solid walls.

molecules are modelled by another L–J potential, which is given by

$$u_{\mathrm{fw}}(r_{ij}) = \begin{cases} 4\varepsilon_{\mathrm{fw}}\left[\left(\frac{\sigma_{\mathrm{fw}}}{r_{ij}}\right)^{12} - c_{\mathrm{fw}}\left(\frac{\sigma_{\mathrm{fw}}}{r_{ij}}\right)^{6}\right] & r_{ij} < r_{\mathrm{c}} \\ 0 & r_{ij} \geq r_{\mathrm{c}} \end{cases} \quad (4)$$

where c_{fw} is a convenient parameter that can be varied to adjust the surface energy. The parameter of wall–fluid interaction, c_{fw}, varied between 0.5 and 1.0, corresponding to the contact angle of fluid atoms and solid walls between $\theta = 140$ and 90°, which is indicated as the hydrophobic and hydrophilic surfaces, respectively [15]. The potential parameters $\varepsilon_{\mathrm{fw}}$ used in the wall–fluid interaction are the same as the fluid–fluid interaction ε_{f}. The diameter of solid atoms σ_{w} are varied to adjust the surface roughness, and the wall–fluid parameter σ_{fw} is determined by $\sigma_{\mathrm{fw}} = (\sigma_{\mathrm{f}} + \sigma_{\mathrm{w}})/2.0$, where σ_{w} is the diameter of wall atom. In order to clearly observe and quantify the degree of slip for a simple fluid flowing through a microchannel, the fluid number density is fixed at 0.288 in all the simulations. The related properties considered in this study are quoted by the reduced unit of the mass of fluid molecule m_{f}; the length of fluid molecule σ_{f}; and the energy of fluid molecule, ε_{f}.

The fluid and wall molecules are initially located at the site of a face-centered cubic lattice. Three layers of wall atoms represent the solid walls and each atom of the wall is anchored at its lattice site by a harmonic restoring force, $\phi_{\mathrm{harm}} = k_{\mathrm{s}}(r_i - r_i^{\mathrm{eq}})^2/2$, where r_i is the position of the wall atom i and r_i^{eq} is the equilibrium position. The spring constant is chosen to be $k_{\mathrm{s}} = 300\varepsilon_{\mathrm{f}}/\sigma_{\mathrm{f}}^2$. The initial velocities of fluid and wall molecules are set randomly according to a given temperature. Both the fluid and wall temperatures were fixed at $T = 1.1\varepsilon_{\mathrm{f}}/k_{\mathrm{B}}$, which is just above the liquid–gas coexistence region for this model. The equations of motion were integrated using the fifth-order Gear predictor–corrector algorithm with a time step of 0.005τ, where $\tau = \sigma_{\mathrm{f}}\sqrt{m_{\mathrm{f}}/\varepsilon_{\mathrm{f}}}$ is the reduced unit of time. At the beginning, the fluid molecules are allowed to move without applying external force. After the thermodynamic equilibrium period of $10^4\tau$, the external force $F_{\mathrm{e}} = 0.1$ is then switched on and the non-equilibrium simulation starts. The work done by the external force is partly converted into heat, which increases the temperature of both the fluid and the wall. To keep the temperature of the system constant, a Gaussian isokinetic thermostat is used to adjust the wall temperature to a constant value at each time step.

3. Hydrodynamics theory

For a planar Stokes flow between two infinite parallel plates, considering an external force applied to the fluid atom in the x direction to drive the flow, the equation of motion in the streaming direction is given by

$$\rho\frac{\mathrm{d}u_x}{\mathrm{d}t} = -\nabla\cdot\mathbf{\Pi} + nF_{\mathrm{e}} \quad (5)$$

where $\mathbf{\Pi}$ is the viscous pressure tensor, u_x is the fluid streaming velocity, ρ is the mass density, n is the fluid number density and F_{e} is the external field. For fluids flowing through microchannels with a external driving force acting on fluid atoms in streaming direction, the magnitude of corresponds to the pressure drop, $\Delta p/L_x$, as used in the hydrodynamic theory of Poiseuille flow. With the assumption of linear constitutive relation relating the shear stress, the Navier–Stokes equation is given by

$$\mu\frac{\mathrm{d}^2u_x}{\mathrm{d}z^2} = -nF_{\mathrm{e}} \quad (6)$$

where μ is the shear viscosity and z is the direction normal to the walls. The boundary conditions with slip occuring at the walls of plates are given by

$$u_x|_{z=h} = u_x|_{z=-h} = u_{\mathrm{slip}} \quad (7)$$

The general solution of equation (6) for Stokes flow is then given by

$$u_x = -\frac{nF_{\mathrm{e}}}{2\bar{\mu}}(z^2 - h^2) + u_{\mathrm{slip}} \quad (8)$$

where $2h$ is the distance between the two plates. Therefore, the volumetric flow rate is calculated by

$$Q = w\int_{-h}^{h} u_x\,\mathrm{d}z = \frac{2wh^3}{3\mu}nF_{\mathrm{e}} + 2wh\cdot u_{\mathrm{slip}} \quad (9)$$

where w is the width of the parallel plates. The first term, $(2wh^3/3\mu)nF_{\mathrm{e}}$, is the theoretical flow rate with a no-slip boundary condition, while the second term, $2whu_{\mathrm{slip}}$, represents an additional flow rate associated with the slip boundary condition.

4. Results and discussions

To investigate the flow behaviors and the dependence of slip length δ on the surface roughness and the attractive wall-fluid interactions, a series of simulations with microsized surface roughness are performed in both hydrophobic and hydrophilic microchannel surfaces. The effect of surface hydrophobicity is characterized by the parameter c_{fw}, while the roughness of the interface is characterized by the parameter σ_{r}. The wall roughness factor, is defined as $\sigma_{\mathrm{r}} = \sigma_{\mathrm{w}}/\sigma_{\mathrm{f}}$. A value of σ_{r} equal to 1.0 indicates a smooth wall surface. To examine the hydrodynamic behaviors of simple fluids passing through hydrophobic and hydrophilic microchannels in a steady state, the long-term average streaming velocity and density profiles are used to quantify the dynamic behaviors and the expansion of fluids, respectively. The computational domain is calculated as a function of z by

dividing the microchannel into bins of width Δz. The average streaming velocity in a specified zth bin is given by $u_x(z) = \sum_{i\in z} m_i u_i(t) / \sum_{i\in z} m_i$, where m_i and u_i are the mass and velocity of the ith atom in the zth bin, and $\sum_{i\in z}$ represents the sum of the fluid atoms occupying zth bin. Similarly, the local average density profiles of the fluids are calculated by $\rho(z) = N_{\text{bin}}(z)/V_z$, where $N_{\text{bin}}(z)$ is the number of fluid atoms occupying in the zth bin of volume V_z. Figure 2 shows the averaged streaming velocity profiles for simple fluid flowing over hydrophilic and hydrophobic microchannels with various wall roughness factors. For a L–J simple fluid molecule, appropriate parameters values for this system are $\varepsilon_f = 121\,\text{K}$ and $\sigma_f = 0.34\,\text{nm}$. The external driving force F_e used in these cases is equal to 0.1. For flow through a hydrophilic microchannel, the velocities are highest in the middle of the channel and smoothly decrease to zero near the wall. This indicates that the no-slip boundary condition is valid for fluid flowing over a hydrophilic surface as shown in figure 2(b). However, the velocity profile has significantly different shapes for a hydrophobic microchannel. The velocity profile has a finite and apparent slip velocity measured above the surface. The magnitude of the slip velocity increases with decreasing the wall roughness factor σ_r. In addition, it is observed that the velocity profiles decrease with σ_r for both the hydrophilic and hydrophobic microchannels. Figure 3 shows the density profiles for a simple fluid flowing over hydrophilic and hydrophobic microchannels with various wall roughness factors. As shown in figures 3(a) and (b), there are peak values near the walls for both hydrophobic and hydrophilic surfaces indicate the fluids form layers. For hydrophilic surfaces, a higher attractive force between fluid and wall molecules induces a higher density layer adjacent to the walls and smooth density profiles in the central regime of the channel. In contrast, for hydrophobic surfaces, the density peak nearest the wall decreases and the magnitude of density profiles in the center are slightly increased. The fluid layer structures are also dependent on

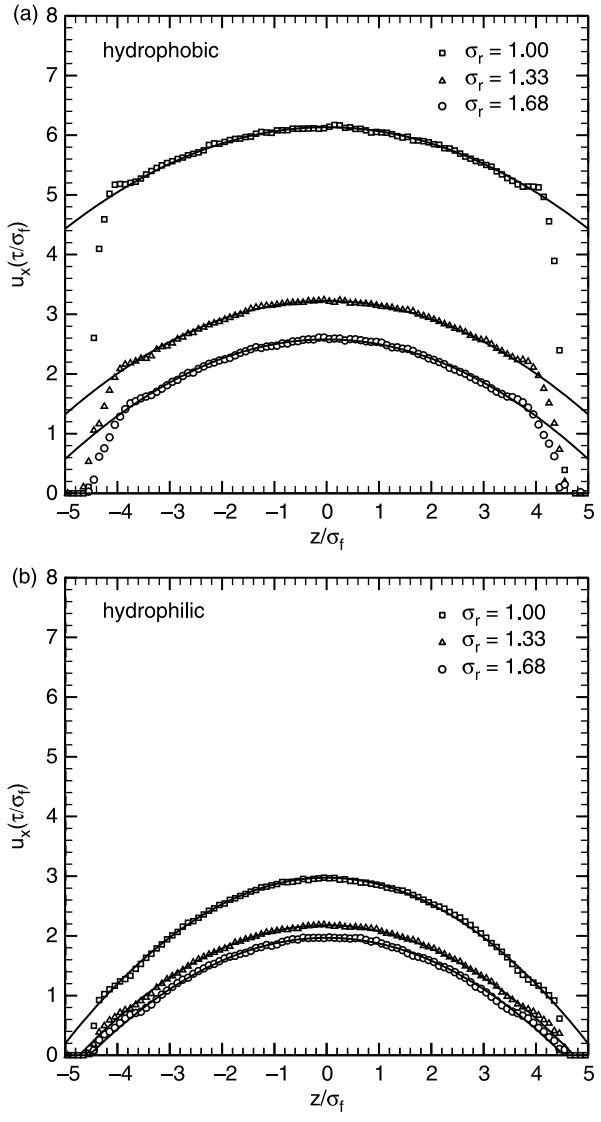

Figure 2. Streaming velocity profiles as a function of z with different values of σ_r (a) hydrophobic surface (b) hydrophilic surface. The solid line indicates the quadratic fitting.

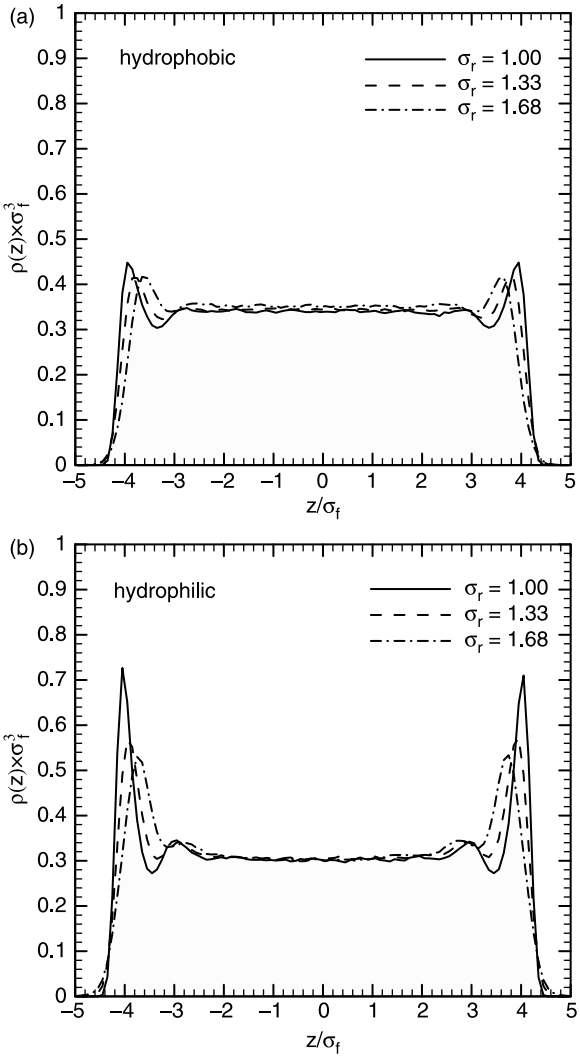

Figure 3. Density profiles as a function of z with different values of σ_r: (a) hydrophobic surface and (b) hydrophilic surface.

the roughness of surface. For a smooth surface ($\sigma_r = 1$), the density profile exhibits a large density oscillations or a strong density layering within the fluid. As σ_r increases, the magnitude of density peak reduces and the fluid layers are shifted towards the central regime. Figure 4 shows the variations of flow rates Q as a function of the number density multiplies by the external driving forces over a wide range of σ_r in both the hydrophobic and hydrophilic microchannels. The theoretical predictions based on a no-slip boundary condition are also applied for comparison. It is observed that the flow rates measured on the hydrophobic surface are larger than those for a hydrophilic surface condition. At a small value of $c_{fw} = 0.5$, corresponding to hydrophobic surface, the weak interaction at wall–fluid interfaces reduces momentum dissipation, resulting in a higher flow rate. However, for the case where $c_{fw} = 1.0$, corresponding to the hydrophilic surface, the attractive interactions between fluid and wall molecules increase the momentum dissipation, leading to a reduction of the flow rate. Moreover, for all of the roughness surfaces tested, the flow rates were found to be significantly less than the smooth cases for both the hydrophobic and hydrophilic surfaces. The flow rates in the hydrophobic microchannel are much larger than the theoretical prediction of Poiseuille flow solution. In comparison, the deviations of flow rate in a hydrophilic surface condition are smaller. Figure 5 shows that the slip velocity u_{slip} varied with the flow rate Q in hydrophobic and hydrophilic surfaces. The measured slip velocity is observed to increase approximately linearly with the flow rate. It is noted a significant slip velocity is found at high flow rate, and the slip velocity disappears as the flow rate below a critical value of $Q = 18\sigma_f^3/\tau$. This is because the degree of slip boundary condition is strongly dependent on slip velocity. When slip velocity is present at the boundaries, the slip length δ is then obtained by fitting the velocity profiles obtained in the simulation according to the analytical prediction deduced from the usual Stokes equation in the bulk fluid, which is given by

$$\left.\frac{\partial u_{slip}}{\partial z}\right|_{z=z_w} = \frac{1}{\delta}\left.u_{slip}\right|_{z=z_w} \tag{10}$$

where u_{slip} is the tangential velocity at the solid surface and z_w is the wall location. The slip length δ as a function of slip velocity u_{slip} is shown in figure 6. There is a linear dependence between the slip length and slip velocity. The slip velocities measured on hydrophobic surfaces are larger than those of hydrophilic surfaces. When the fluid molecules approach the hydrophilic surface, the fluid molecules have a tendency to be absorbed onto the surface and lose a considerable portion of drift velocity or the tangential momentum, resulting in the reduction of slip velocity above the surface. The influences of surface roughness on the boundary slip are then quantitatively examined in the following. Figure 7 shows the dependence of slip length on the surface roughness for both hydrophobic and hydrophilic surfaces. It can be observed

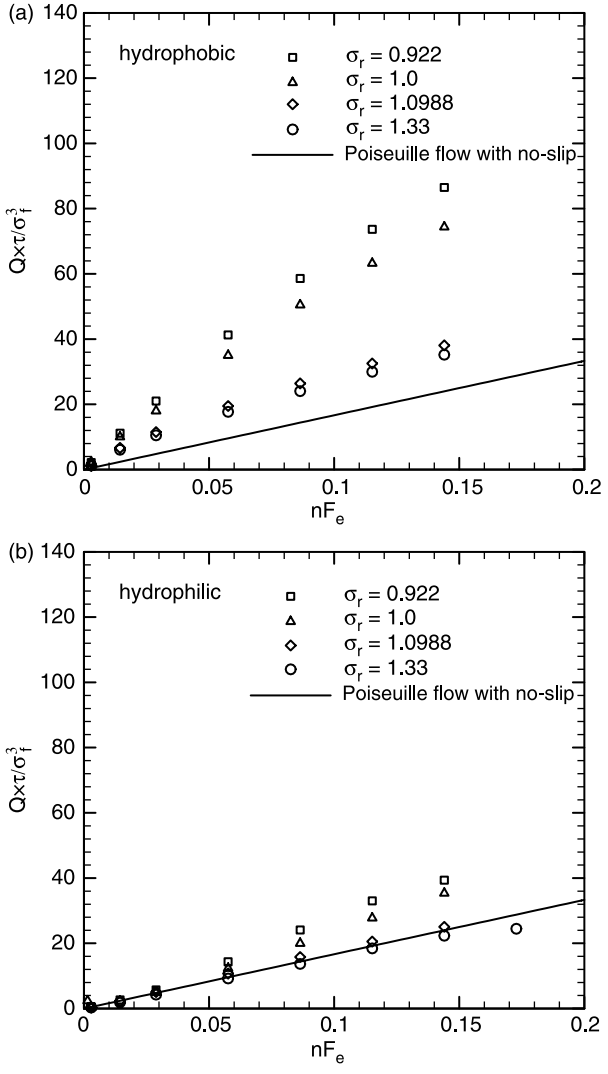

Figure 4. Flow rate Q as a function of nF_e over a wide range of σ_r: (a) hydrophobic surface and (b) hydrophilic surface.

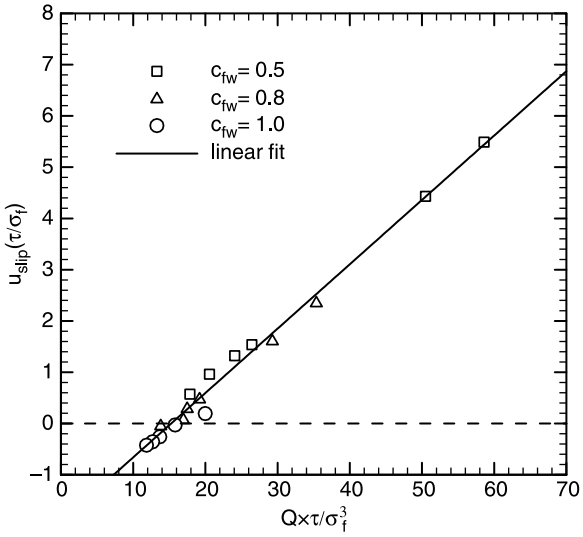

Figure 5. Slip length δ varies with the flow rate Q for hydrophilic and hydrophobic surfaces.

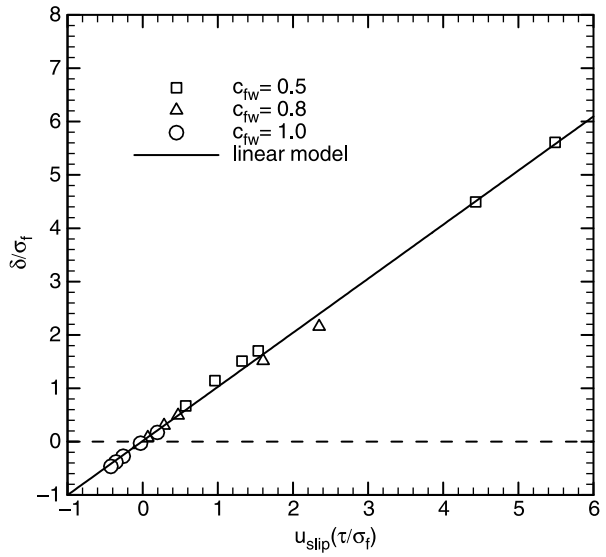

Figure 6. Slip length δ varies with the slip velocity u_{slip} for hydrophilic and hydrophobic surfaces.

that the magnitudes of slip length in hydrophilic surface conditions are much smaller than those in hydrophobic surfaces. The degree of slip length decreases with the presence of surface roughness for both the hydrophobic and the hydrophilic surfaces. For hydrophobic surfaces ($c_{fw} = 0.5$), a significant boundary slip is found for both smooth and rough surfaces. However, for intermediate and hydrophilic surface ($c_{fw} = 0.8$ and 1.0), the slip boundary condition is only found on smooth surfaces ($\sigma_r < 1.0$), and a stick boundary condition is observed on rough surfaces ($\sigma_r > 1.0$). A large value of σ_r implies a large area of fluid–wall interface and a higher friction at the interface, resulting in a reduction of slip length. In addition, the fluid molecules flowing over a rough surface lose more tangential momentum than those flowing over smoother surfaces, resulting in the reduction of slip velocity and slip length for both the hydrophobic and hydrophilic surfaces. Sokhan *et al.* [23] analyzed the difference between the molecular velocities before and after the collisions to determine the Maxwell coefficient of slip in nanopores. They showed that the slip coefficients were determined by the fluid–fluid attraction and the normal pressure in the fluid for different fluid densities. In the current studies, the variations of the normal pressure to the surface are not apparent as σ_r varies. This indicates that the influence of the normal pressure on the slip length seems to be not important in these cases. The variations of slip length as a function of shear rate $\dot{\gamma}$ in a logarithm scale for hydrophobic and hydrophilic surfaces are shown in figure 8. For hydrophobic surfaces, the simulation results show that the slip length increases linearly with shear rate for both the smooth and rough surfaces. The apparent fluid slip observed at a hydrophobic surface may be due to the presence of nanobubbles or a low fluid density layer forming a gap near the solid surface. The nucleation of bubbles reduces the momentum dissipation between fluid and wall atoms, resulting in the increase of boundary slip

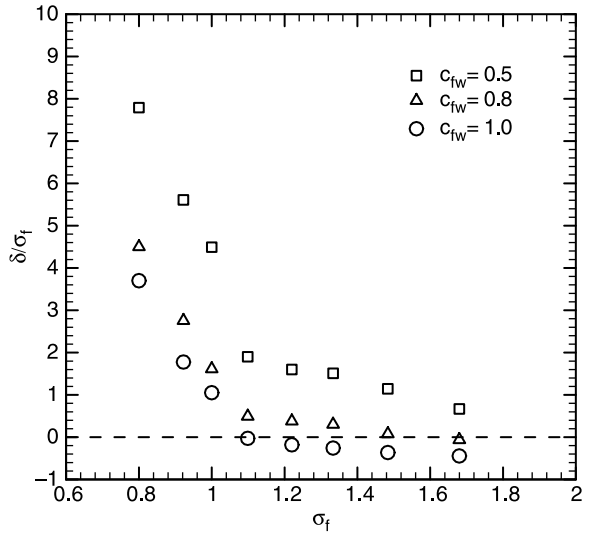

Figure 7. Dependence of slip length on surface roughness for hydrophobic and hydrophilic surfaces.

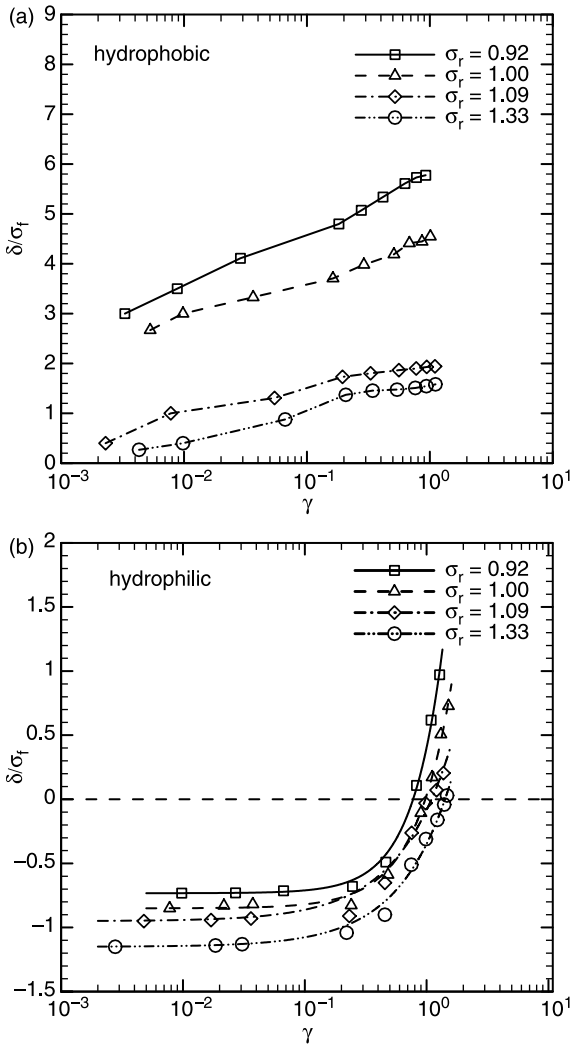

Figure 8. Variations of slip length as a function of $\dot{\gamma}$ in a logarithm scale: (a) hydrophobic surface and (b) hydrophilic surface.

rapidly. In comparison, the slip length exhibits different shapes for fluid over hydrophilic surfaces. At low shear rate, the slip length is negative and nearly constant in both the smooth and roughness surface conditions. This indicates that the no slip condition is observed for flow on hydrophilic surfaces at low shear rate. Beyond a critical shear rate of $\dot{\gamma} \cong 1.0$, the slip length is observed to increase rapidly with $\dot{\gamma}$. The slip boundary condition model proposed by Navier [24] stated that the slip velocity at the wall–fluid interface is proportional to the shear rate. Employing MD simulation, Thompson and Troian [13] showed that the slip length for Newtonian fluids in Couette flow had a power law dependence on the shear rate according to $L_s = L_s^*(1 - \dot{\gamma}/\dot{\gamma}_c)^{-1/2}$. Following the slip model proposed by Thompson and Troian, a power dependence on shear rate of $\delta = A(1 - \dot{\gamma})^B$ is fitting to the simulation data over hydrophilic surface. The values of parameters A and B are listed in table 1.

5. Conclusion

Using MD simulation, the hydrodynamic behaviors and slip phenomena of simple fluids flowing over solid surfaces in a microchannel are examined in this study. The smooth and rough surfaces at an atomic scale are considered with either hydrophilic or hydrophobic boundary conditions. The simulation results show that the slip boundary conditions strongly depend on both the attractive wall–fluid interaction, surface roughness and the shear rate near the surface. The degree of slip is severely suppressed by surface roughness for both hydrophilic and hydrophobic surfaces. The degree of wall slip is also strongly dependent on the shear rate. For a simple fluid flowing over a hydrophobic surface, the slip length increases linearly with shear rate for both the smooth and the rough surfaces. The presence of nanobubbles or a low fluid density layer on the hydrophobic surface reduces the momentum dissipation between fluid and wall atoms, thereby resulting in a rapidly increase of boundary slip. For the case of a hydrophilic surface, the no-slip boundary is observed at low shear rate for both the smooth and rough surface conditions. Beyond a critical shear rate, the slip length is observed to increase rapidly.

Table 1. The values of A and B in the power law dependence $\delta = A(1 - \dot{\gamma})^B$.

Wall roughness factor σ_r	A	B
0.90	1.1353	−1.7178
1.00	0.8813	−1.4574
1.09	0.8668	−0.9909
1.33	0.8021	−1.0367

References

[1] R. Pit, H. Hervet, L. Leger. Direct experimental evidence of slip in hexadecane: solid interfaces. *Phys. Rev. Lett.*, **85**, 980 (2000).
[2] Y. Zhu, S. Granick. Rate-dependent slip of Newtonian liquid at smooth surface. *Phys. Rev. Lett.*, **87**, 096105 (2001).
[3] V.S.J. Craig, C. Neto, D.R.M. Williams. Shear-dependent boundary slip in an aqueous newtonian liquid. *Phys. Rev. Lett.*, **87**, 054504 (2001).
[4] D.C. Tretheway, C.D. Meinhart. Apparent fluid slip at hydrophobic microchannel walls. *Phys. Fluids*, **14**, L9 (2002).
[5] J. Tyrell, P. Attard. Images of nanobubbles on hydrophobic surfaces and their interactions. *Phys. Rev. Lett.*, **87**, 176104 (2001).
[6] Y. Zhu, S. Granick. Limits of the hydrodynamic no-slip boundary condition. *Phys. Rev. Lett.*, **88**, 106102 (2002).
[7] E. Bonaccurso, M. Kappl, H.J. Butt. Hydrodynamic force measurements: boundary slip of water on hydrophilic surfaces and electrokinetic effects. *Phys. Rev. Lett.*, **88**, 076103 (2002).
[8] E. Bonaccurso, H.J. Butt, V.S.J. Craig. Surface roughness and hydrodynamic boundary slip of a Newtonian fluid in a completely wetting system. *Phys. Rev. Lett.*, **90**, 144501 (2003).
[9] C.H. Choi, K. Johan, A. Westin, K.S. Breuer. Apparent slip flows in hydrophilic and hydrophobic microchannels. *Phys. Fluids*, **15**, 2897 (2003).
[10] C. Cottin-Bizonne, S. Jurine, J. Baudry, J. Crassous, F. Restagno, E. Charlaix. Nanorheology: an investigation of the boundary condition at hydrophobic and hydrophilic interfaces. *Eur. Phys. J. E*, **9**, 47 (2003).
[11] R. Steitz, T. Gutberlet, T. Hauss, B. Klosgen, R. Krastev, S. Schemmel, A.C. Simonsen, G.H. Findenegg. Nanobubbles and their precursor layer at the interface of water against a hydrophobic surface. *Langmuir*, **19**, 2409 (2003).
[12] P.A. Thompson, M.O. Robbins. Shear flow near solids: epitaxial order and flow boundary conditions. *Phys. Rev. A*, **41**, 6830 (1990).
[13] P.A. Thompson, S.M. Troian. A general boundary condition for liquid flow at solid surfaces. *Nature*, **389**, 360 (1997).
[14] J.L. Barrat, L. Bocquet. Large slip effect at a nonwetting fluid–solid interface. *Phys. Rev. Lett.*, **82**, 4671 (1999).
[15] K.P. Travis, K.E. Gubbins. Poiseuille flow of Lennard–Jones fluids in narrow slit pores. *J. Chem. Phys.*, **112**, 1984 (2000).
[16] A. Jabbarzadeh, J.D. Atkinson, R.I. Tanner. Effect of the wall roughness on slip and rheological properties of hexadecane in molecular dynamics simulation of Couette shear flow between two sinusoidal walls. *Phys. Rev. E*, **61**, 690 (2000).
[17] M. Cieplak, J. Koplik, J.R. Banavar. Boundary conditions at a fluid–solid interface. *Phys. Rev. Lett.*, **86**, 803 (2001).
[18] C. Cottin-Bizonne, E. Charlaix, L. Bocquet, J-L. Barrat. Low-friction flows of liquid at nanopatterned interfaces. *Nat. Mater.*, **2**, 238 (2003).
[19] V.P. Sokhan, D. Nicholson, N. Quirke. Fluid flow in nanopores: an examination of hydrodynamic boundary conditions. *J. Chem. Phys.*, **115**, 3878 (2001).
[20] S. Richardson. On the no-slip boundary condition. *J. Fluid Mech.*, **59**, 707 (1973).
[21] N.V. Priezjev, S.M. Troian. Molecular origin and dynamic behavior of slip in sheared polymer films. *Phys. Rev. Lett.*, **92**, 018302 (2004).
[22] T.M. Galea, P. Attard. Molecular dynamics study of the effect of atomic roughness on the slip length at the fluid–solid boundary during shear flow. *Langmuir*, **20**, 3477 (2004).
[23] V.P. Sokhan, N. Quirke. Interfacial friction and collective diffusion in nanopores. *Mol. Sim.*, **30**, 217 (2004).
[24] C.L.M.H. Navier. Mémoire sur le lois du mouvement des fluids. *Mém. Acad. Roy. Sci. Paris*, **6**, 389 (1823).